Microstructure studies of amorphous and nanocrystalline (Fe$_{1-x}$Co$_x$)$_{85.4}$Zr$_{6.8-y}$M$_y$B$_{6.8}$Cu$_1$ (*x* = 0 or 0.1, *y* = 0 or 1, M = Mo, Nb or Nd) alloys

Jacek Olszewski,
Józef Zbroszczyk,
Hirotoshi Fukunaga,
Wanda Ciurzyńska,
Jan Świerczek,
Mariusz Hasiak,
Kamila Perduta,
Agnieszka Łukiewska,
Alina Młyńczyk

Abstract The amorphous and nanocrystalline (Fe$_{1-x}$Co$_x$)$_{85.4}$Zr$_{6.8-y}$M$_y$B$_{6.8}$Cu$_1$ (x = 0 or 0.1, y = 0 or 1, M = Mo, Nb or Nd) alloys were studied using Mössbauer spectroscopy. We have stated that after the low temperature annealing of the samples the decrease of the average hyperfine field due to the Invar effect was observed. This effect is associated with the increase of atom packing density after the annealing of the samples, which may lead to the noncolinear spin state in some regions. This phenomenon was completely suppressed after substitution of 10% of Fe atoms by Co atoms. At early stages of crystallization of the Fe$_{85.4}$Zr$_{6.8-y}$M$_y$B$_{6.8}$Cu$_1$ (y = 0 or 1, M = Mo, Nb or Nd) alloys, the interfacial zone is poor in iron due to diffusion of Zr, B, Nb, Mo and Nd atoms outside regions where α-Fe fine grains are created. However, the iron content in the amorphous matrix is the same as in the as-quenched state. The iron concentration in the interfacial zone of the nanocrystalline alloys obtained by the accumulative annealing depends on the chemical composition of the as-quenched samples. In the nanocrystalline samples obtained by two-step annealing, the iron content in the interfacial layer is higher than in the amorphous matrix.

Key words Invar effect • nanocrystalline alloys • interfacial zone

J. Olszewski$^{\boxtimes}$, J. Zbroszczyk, W. Ciurzyńska, J. Świerczek,
M. Hasiak, K. Perduta, A. Łukiewska, A. Młyńczyk
Institute of Physics,
Częstochowa University of Technology,
19 Armii Krajowej Ave., 42-200 Częstochowa, Poland,
Tel.: +48 34/ 325 07 96, Fax: +48 34/ 325 07 95,
e-mail: jacek@mim.pcz.czest.pl

H. Fukunaga
Faculty of Engineering,
Nagasaki University,
Nagasaki 852-8521, Japan

Introduction

Fe-Zr-based amorphous alloys are very interesting because of their anomalous physical properties such as low and almost independent of temperature thermal expansion and Young modulus, large values of high field susceptibility and forced volume magnetostriction, and large negative pressure effect on the magnetization and on the Curie temperature. These properties are characteristic of Invar materials [4, 7, 11–13]. These anomalies may be connected with distribution of Fe-Fe nearest neighbour distances in Fe-Zr-based alloys which involves the competition between ferro- and antiferromagnetic interactions. One of the most powerful methods for structure investigations of amorphous and nanocrystalline alloys is Mössbauer spectroscopy [8]. Fe-Zr-based amorphous alloys crystallize in two stages [1]. The first stage involves the precipitation of α-Fe fine grains in the amorphous phase. During the second stage the growth of α-Fe grains and formation of intermetallic phases are observed. The nanocrystalline materials produced by utilizing the first stage of crystallization show excellent soft magnetic properties such as the high initial susceptibility and low coercivity accompanied by high saturation magnetization [9]. The superior soft magnetic properties of these materials are related to their structure, i.e. fine α-Fe grains embedded in the residual amorphous phase which exhibits highly disordered structure [5, 6]. One can distinguish in that phase two components: the interfacial zone and the amorphous matrix. Beside excellent soft magnetic properties, these nanocrystalline materials are interesting objects for

basic research. The majority of investigations was performed for the amorphous and nanocrystalline Fe-Zr-B-Cu alloys.

In this paper, we present microstructure studies of amorphous and nanocrystalline $(Fe_{1-x}Co_x)_{85.4}Zr_{6.8-y}M_yB_{6.8}Cu_1$ ($x = 0$ or 0.1, $y = 0$ or 1, M = Mo, Nb or Nd) alloys.

Experimental procedure

The amorphous $(Fe_{1-x}Co_x)_{85.4}Zr_{6.8-y}M_yB_{6.8}Cu_1$ ($x = 0$ or 0.1, $y = 0$ or 1, M = Mo, Nb or Nd) alloys in the form of ribbons with the thickness of 0.02 mm and the width of 2 mm were prepared by a melt spinning technique in an argon protective atmosphere. The crystallization temperatures of the as-quenched samples were found from DSC curves recorded at the heating rate of 10 K/min using a Netzsch STA 409 C differential scanning calorimeter. The microstructure of the amorphous and partially crystallized samples was investigated by Mössbauer spectroscopy and transmission electron microscopy. The transmission Mössbauer spectra were measured at room temperature by a conventional constant acceleration spectrometer with the $^{57}Co(Rh)$ source of about 50 mCi activity. The experimental spectra fittings were performed with the NORMOS package developed by Brand [2]. From Mössbauer data, under assumption of the same probability of recoil free absorption of γ radiation in different phases and taking into account the dependence of hyperfine field and isomer shift on Co concentration in α-FeCo phase, the phase composition and iron content in all components were evaluated [3]. The iron concentration in the interfacial zone of the nanocrystalline $Fe_{85.4}Zr_{6.8-y}M_yB_{6.8}Cu_1$ ($y = 0$ or 1, M = Mo, Nb or Nd) alloys was determined under the assumption that the dependence of the average hyperfine field on iron concentration is the same as in the crystalline phase. However, the iron concentration in amorphous matrix (Fe_m) was determined using the equation: $Fe_m = (R_mC_{Fe})/(R_{tot}V_m)$ where R_m and R_{tot} are the relative areas of amorphous subspectra corresponding to the amorphous matrix and total area of the spectrum, respectively. C_{Fe} is the percentage iron concentration in the as-quenched alloys and V_m is the volume fraction of the amorphous matrix [3]. The electron microscopy studies were carried out for the samples in the form of discs, 3 mm in diameter, after ion milling. In order to avoid the composition fluctuation along the ribbon length, we investigated the samples subjected to the accumulative annealing. We studied two sets of the samples. The first one was annealed at 573 K for 1 h and then for 40 and 30 min at 723 K and at 800 K for 5 min and finally at 808 K for 10 min. The second set of the samples was heated for 1 h at 673 K and then at 810 K. Moreover, the Mössbauer spectroscopy studies were additionally carried out for the samples annealed at 573 K for different times.

Results and discussion

All investigated alloys in the as-quenched state were fully amorphous as it was confirmed by Mössbauer spectroscopy investigations. In Fig. 1, some Mössbauer spectra and the corresponding hyperfine field distributions of the as-quenched samples are shown. It is seen that the spectra are asymmetric and consist of broad and overlapped lines
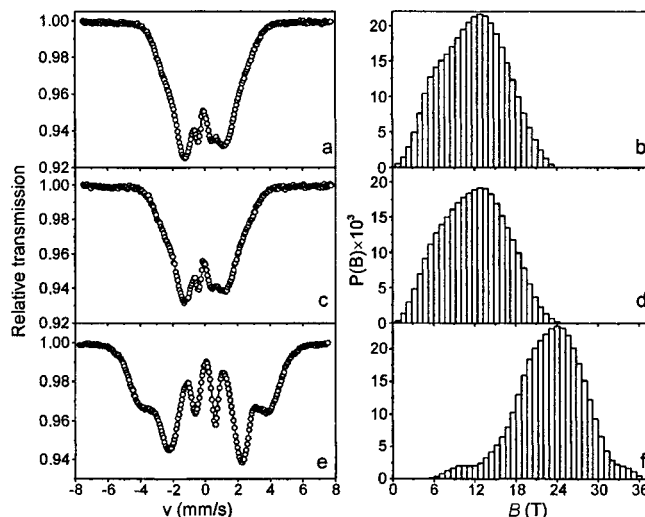

Fig. 1. Mössbauer spectra (a, c, e) and corresponding hyperfine field distributions (b, d, f) of the $(Fe_{1-x}Co_x)_{85.4}Zr_{6.8-y}Nb_yB_{6.8}Cu_1$ alloys in the as-quenched state: $x = 0$, $y = 0$ (a, b); $x = 0$, $y = 1$ (c, d); $x = 0.1$, $y = 1$ (e, f).

that are characteristic of the amorphous state. We have stated that after annealing of the as-quenched $Fe_{85.4}Zr_{6.8-y}M_yB_{6.8}Cu_1$ ($y = 0$ or 1, M = Mo, Nb or Nd) alloys at 573 K, the decrease of the average hyperfine field occurs (Table 1). This behaviour is the most distinct in the alloys containing Mo and Nd and may be explained by the Invar effect [8]. As an example, in Fig. 2, the Mössbauer spectra and corresponding hyperfine field distributions of the as-quenched $Fe_{85.4}Zr_{5.8}Mo_1B_{6.8}Cu_1$ and annealed alloy at 573 K for different times are shown. It is seen (Fig. 2) that the hyperfine field distributions exhibit the bimodal profile
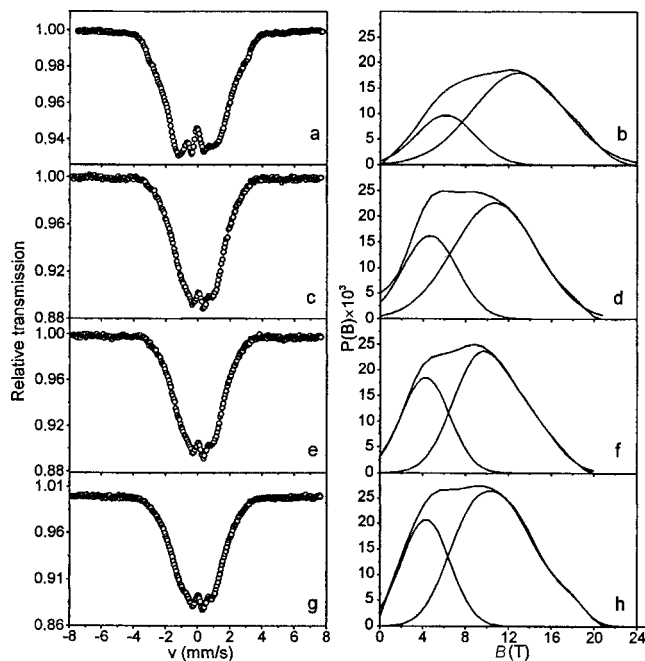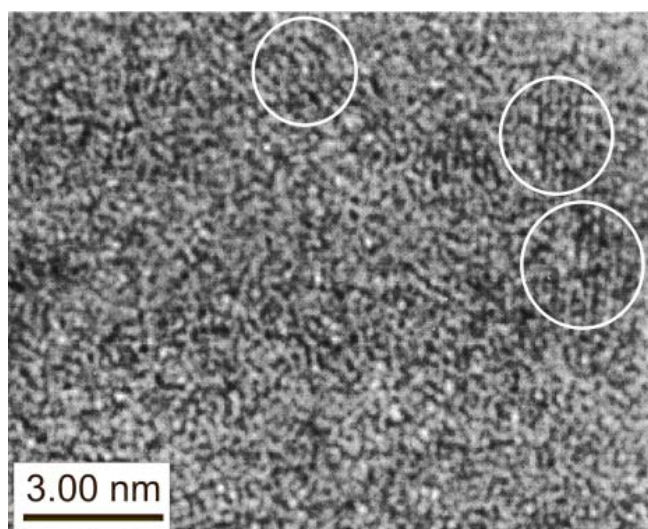

Fig. 2. Mössbauer spectra (a, c, e, g) and corresponding hyperfine field distributions (b, d, f, h) with marked low and high field components of the $Fe_{85.4}Zr_{5.8}Mo_1B_{6.8}Cu_1$ alloy in the as-quenched state (a, b) and annealed at 573 K for 30 min (c, d), 1 h (e, f) and 2 h (g, h).

Table 1. Average hyperfine field (B_{eff}) and width of hyperfine field distributions (ΔB) for the amorphous $(Fe_{1-x}Co_x)_{85.4}Zr_{6.8-y}M_yB_{6.8}Cu_1$ ($x = 0$ or 0.1, $y = 0$ or 1, M = Mo, Nb or Nd) alloys in the as-quenched state and after annealing at 573 K and 673 K.

Samples	$x = 0, y = 0$		$x = 0, y = 1$ M = Nb		$x = 0, y = 1$ M = Mo		$x = 0, y = 1$ M = Nd		$x = 0.1, y = 1$ M = Nb	
Heat treatment	B_{eff}(T)	ΔB(T)	B_{eff}(T)	ΔB(T)	B_{eff}(T)	ΔB(T)	B_{eff}(T)	ΔB(T)	B_{eff}(T)	ΔB(T)
As-quenched	11.88	4.56	11.82	4.62	10.34	4.61	10.10	4.46	22.89	5.04
573 K/30 min	–	–	–	–	8.78	4.36	8.73	4.16	–	–
573 K/1 h	11.21	4.51	10.87	4.56	8.45	4.17	8.79	4.18	22.81	5.36
573 K/2 h	–	–	–	–	8.95	4.44	9.11	4.36	–	–
673 K/1 h	12.39	4.74	12.28	4.86	10.25	4.77	10.39	4.64	–	–

indicating the presence of two different Fe-sites. The low field component in the hyperfine field distributions corresponds to Fe-rich regions with small Fe-Fe distances which are responsible for Invar anomalies in this alloy, whereas the high-field component is attributed to Fe atoms which in their nearest neighbourhood have also Zr and B atoms [11]. After the annealing of the sample at 573 K, the contribution of low field component increases (Fig. 2). It is commonly known that annealing of the amorphous materials below the crystallization temperature leads to the enhancement of the atom packing density which involves the decrease of the Fe-Fe nearest neighbour distances in the investigated alloys. As a result, the weakness of the ferromagnetic coupling between Fe-Fe atoms and the decrease of the hyperfine field of the low-field component occur. The increase of the low-field component contribution and its hyperfine field decrease explain the decrease of the average hyperfine field after the annealing of the samples (Table 1). In Table 1, the width of the hyperfine field distribution, ΔB, is also presented, which may be treated as a measure of a number of nonequivalent Fe sites. However, after the heat treatment of the samples at 673 K for 1 h, the increase of the average hyperfine field occurs. It may be connected with nucleation of α-Fe grains. One can see in Fig. 3 atomic medium-range order as a local atomic arrangement in some regions of the sample. These areas may be treated as the

nuclei of the crystalline α-Fe phase [10]. It is worth noticing that after the replacement of 10% of Fe atoms by Co atoms in the investigated alloys, the Invar effect is completely
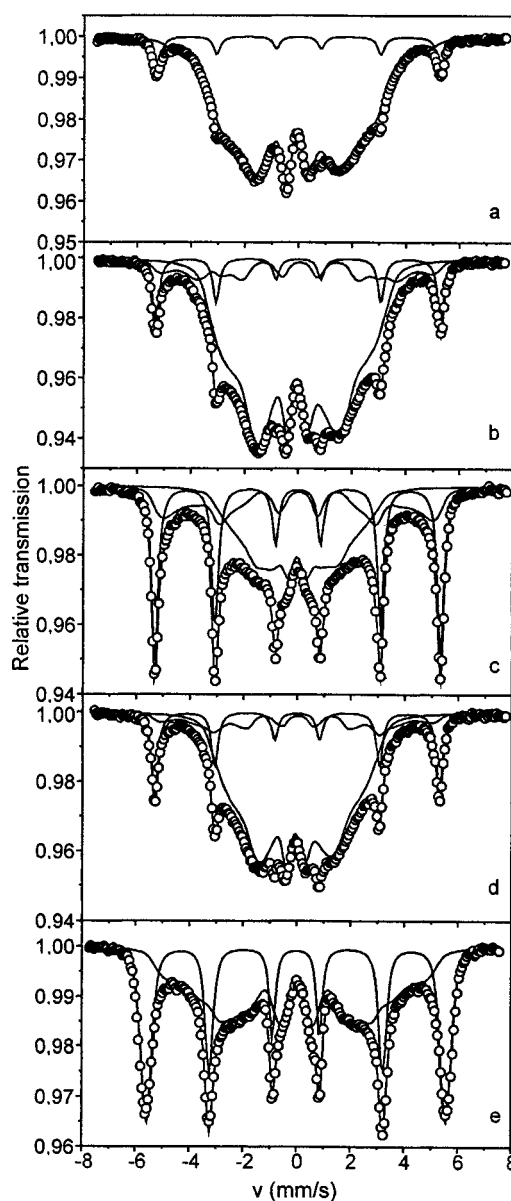

Fig. 3. Micrograph of the amorphous $Fe_{85.4}Zr_{5.8}Mo_1B_{6.8}Cu_1$ alloy annealed at 673 K for 1 h obtained by a high resolution electron microscope (nuclei are indicated by circles).

Fig. 4. Mössbauer spectra of the $(Fe_{1-x}Co_x)_{85.4}Zr_{6.8-y}M_yB_{6.8}Cu_1$ alloys annealed at 573 K for 1 h and then at 723 K for 40 min: $x = 0$, $y = 0$ (a); $x = 0$, $y = 1$, M = Nb (b); $x = 0$, $y = 1$, M = Mo (c); $x = 0$, $y = 1$, M = Nd (d); $x = 0.1$, $y = 1$, M = Nb (e).

Table 2. Volume fractions of amorphous matrix (V_m), interfacial zone (V_{int}), crystalline phase (V_{cr}) and corresponding iron content in those phases (Fe_m), (Fe_{int}) and (Fe_{cr}) in the nanocrystalline $(Fe_{1-x}Co_x)_{85.4}Zr_{6.8-y}M_yB_{6.8}Cu_1$ ($x = 0$ or 0.1, $y = 0$ or 1, M = Mo, Nb or Nd) alloys.

Heat treatment	Samples	Fe_m (at.%)	V_m	Fe_{int} (at.%)	V_{int}	Fe_{cr} (at.%)	V_{cr}
573 K/1 h	$x = 0, y = 0$	85.4	0.87	68.0	0.08	95.0	0.05
+ 723 K/40 min	$x = 0,\ y = 1$, M = Nb	85.4	0.81	69.0	0.10	98.0	0.09
	$x = 0,\ y = 1$, M = Mo	85.4	0.42	72.8	0.31	100	0.27
	$x = 0,\ y = 1$, M = Nd	85.4	0.78	68.0	0.10	99.0	0.12
	$x = 0.1, y = 1$, M = Nb	–	–	–	–	95.0	0.37
573 K/1 h	$x = 0, y = 0$	79.3	0.32	75.6	0.31	100	0.37
+723 K/40 min	$x = 0,\ y = 1$, M = Nb	79.7	0.30	75.9	0.34	100	0.37
+723 K/30 min	$x = 0,\ y = 1$, M = Mo	75.7	0.28	77.3	0.35	100	0.37
+800 K/5 min	$x = 0,\ y = 1$, M = Nd	75.1	0.25	76.5	0.35	100	0.40
+808 K/10 min							
673 K/1 h	$x = 0, y = 0$	72.9	0.25	76.0	0.32	100	0.43
+810 K/1 h	$x = 0,\ y = 1$, M = Nb	70.9	0.26	76.5	0.33	100	0.41
	$x = 0,\ y = 1$, M = Mo	71.4	0.25	78.0	0.34	100	0.41
	$x = 0,\ y = 1$, M = Nd	68.3	0.23	76.5	0.32	100	0.45

suppressed (Table 1). This effect might be explained by assuming that Fe-Co exchange interaction is larger than Fe-Fe couples. It involves the stabilization of the spin structure and is responsible for the enhancement of the average hyperfine field (B_{eff}).

In the Mössbauer spectra of the nanocrystalline $Fe_{85.4}Zr_{6.8-y}M_yB_{6.8}Cu_1$ ($y = 0$ or 1, M = Mo, Nb or Nd) samples (Fig. 4) it is seen one well-resolved sextet of sharp lines ascribed to α-Fe phase superimposed on broad lines connected with the intergranual amorphous phase. The hyperfine field of the crystalline phase at early stages of crystallization is slightly lower than for pure α-iron (33.00 T) which indicates that the crystalline grains contain small amount of non-magnetic impurities such as B and Zr. However, in the nanocrystalline $(Fe_{1-x}Co_x)_{85.4}Zr_{5.8}Nb_1B_{6.8}Cu_1$ ($x = 0.1$) alloy the disordered α-FeCo phase with fine grains was found. The value of the hyperfine field of this crystalline phase (33.68 T) indicates that it contains 5% of Co atoms.

Moreover, from Mössbauer spectra analysis, it has been found that at early stages of the crystallization of the $Fe_{85.4}Zr_{6.8-y}M_yB_{6.8}Cu_1$ ($y = 0$ or 1, M = Mo, Nb or Nd) alloy (after the heat treatment at 573 K for 1 h and then at 723 K for 40 min) the iron content in the amorphous matrix is the same as in the as-received samples. However, the interfacial zone is poorer in iron than the amorphous matrix. It is caused by the diffusion of insoluble in α-Fe phase atoms outside regions where crystalline grains grow. From DSC studies, we have found that the temperature of 723 K is well below the optimum crystallization temperature (800 K). Therefore, the appearance of α-Fe phase after that treatment may be connected with growth of the crystalline grains from nuclei frozen in the samples during the rapid quenching. The volume fractions of the crystalline phase and interfacial zone increase with the annealing time and temperature (Table 2). It is seen that the amorphous matrix in nanocrystalline alloys is depleted in iron in comparison with the as-quenched state due to precipitation of α-Fe grains. Moreover, the iron concentration in the interfacial zone of the nanocrystalline $Fe_{85.4}Zr_{6.8}B_{6.8}Cu_1$ and $Fe_{85.4}Zr_{5.8}Nb_1B_{6.8}Cu_1$ alloys (obtained by the accumulative annealing of the amorphous samples at 573 K and then at

723 K, 800 K and 808 K) is lower than in the amorphous matrix. This may be connected with diffusion of Zr and B atoms trapped in α-Fe phase during early stages of crystallization (Table 2). It leads to an increase of the iron concentration in that phase with annealing time and temperature (Table 2). This effect has not been observed in samples containing Mo and Nd and after two-step heat treatment at 673 K and 810 K of the investigated alloys. The obtained results indicate that the iron concentration in the interfacial zone depends on the annealing conditions and chemical compositions of the samples.

Conclusions

- In the amorphous samples annealed below the crystallization temperature (573 K) the decrease of the average hyperfine field is observed.
- The replacement of 10% of Fe atoms by Co atoms leads to two-fold enhancement of the average hyperfine field and suppressing of the Invar effect.
- At early stages of crystallization the iron content in the amorphous matrix is the same as in the as-quenched state.
- The iron concentration in the interfacial layer of the nanocrystalline alloys depends on the chemical composition of the as-quenched alloys and annealing conditions.

References

1. Al-Haj M, Barry J (1998) Nanocrystallization kinetics of $Fe_{85.5}Zr_4Nb_4B_{5.5}Al_1$ amorphous alloys. J Mater Sci Lett 17:1125–1127
2. Brand RA (1987) Improving the validity of hyperfine field distributions from magnetic alloys. Nucl Instrum Meth Phys Res B 28:398–416

3. Ciurzyńska WH, Varga LK, Olszewski J, Zbroszczyk J, Hasiak M (2000) Mössbauer studies and some magnetic properties of amorphous and nanocrystalline $Fe_{87-x}Zr_7B_6Cu_x$ alloys. J Magn Magn Mater 208:61–68

4. Fernández Barguín L, Gómez Sal JC, Gorria P, Gariataonandia JS, Barandiarán JM (2003) Reentrant spin-glass behavior in Fe-Zr-B amorphous alloys. J Non-Cryst Solids 329:94–99

5. Grenèche JM, Miglierini M, Ślawska-Waniewska A (2000) Iron-based nanocrystalline alloys investigated by ^{57}Fe Mössbauer spectrometry. Hyperfine Interact 126:27–34

6. Kopcewicz M, Grabias A, Williamson DL (1997) Magnetism and nanostructure of $Fe_{93-x-y}Zr_7B_xCu_y$ alloys. J Appl Phys 82;4:1747–1758

7. Krey U, Krauss U, Krompiewski S (1992) Itinerant spin glass states and asperomagnetism of amorphous Fe and iron-rich Fe/Zr alloys. Magn Magn Mater 103:37–46

8. Makarov VA, Belenkii AY, Kozlova OS (1993) Hyperfine field distribution, Invar anomalies in amorphous Fe-Zr alloys, and problems of amorphous Fe magnetism. Phys Status Solidi A 139:173–179

9. Makino A, Hatanai T, Inoue A, Masumoto T (1997) Nanocrystalline soft magnetic Fe-M-B (M = Zr, Hf, Nb) alloys and their applications. Mater Sci Eng A 226/228:594–602

10. Nakamura M, Hirotsu Y, Anazawa K, Makino A, Inoue A, Masumoto T (1994) High resolution electron microscopy study of microstructural changes in magnetic Fe-Nb-B films in the course of annealing. Mater Sci Eng A 179/180:487–490

11. Roig A, Ślawska-Waniewska A, Molins E (1998) Magnetic hyperfine fields in FeZrB amorphous alloys. J Phys IV France 8:Pr2-87–Pr2-90

12. Ślawska-Waniewska A, Żuberek R (1996) Magnetic properties of FeZrB(Cu) amorphous alloys; the effect of boron content. J Magn Magn Mater 160:253–254

13. Tange H, Matsuyama T, Chikazawa A, Konishi K, Kamimori T (1998) Spin glass and Invar effect for Fe(ZrB) amorphous alloys. J Magn Magn Mater 177/181:125–126